



Small-molecule inhibition of the uPAR·uPA interaction: Synthesis, biochemical, cellular, in vivo pharmacokinetics and efficacy studies in breast cancer metastasis

Timmy Mani^a, Fang Wang^a, William Eric Knabe^a, Anthony L. Sinn^{c,d}, May Khanna^a, Inha Jo^a, George E. Sandusky^{i,j}, George W. Sledge Jr.^{b,c,e}, David R. Jones^b, Rajesh Khanna^h, Karen E. Pollok^{c,d}, Samy O. Meroueh^{a,e,f,g,h,*}

^a Department of Biochemistry and Molecular Biology, Indiana University School of Medicine, Van Nuys Medical Science Building, MS 4023, 635 Barnhill Drive, Indianapolis, IN 46202-5122, USA

^b Department of Medicine, Indiana University School of Medicine, Indianapolis, IN 46202, USA

^c Herman B Wells Center for Pediatric Research, Indiana University School of Medicine, Indianapolis, IN 46202, USA

^d In vivo Therapeutics Core, Indiana University School of Medicine, Indianapolis, IN 46202, USA

^e Indiana University Cancer Center, Indiana University School of Medicine, Indianapolis, IN 46202, USA

^f Center for Computational Biology and Bioinformatics, Indiana University School of Medicine, Indianapolis, IN 46202, USA

^g Department of Chemistry and Chemical Biology (IUPUI), Indiana University School of Medicine, Indianapolis, IN 46202, USA

^h Stark Neurosciences Research Institute, Indiana University School of Medicine, Indianapolis, IN 46202, USA

ⁱ Department of Surgery, Indiana University School of Medicine, Indianapolis, IN 46202, USA

^j Department of Pathology and Laboratory Medicine, Indiana University School of Medicine, Indianapolis, IN 46202, USA

ARTICLE INFO

Article history:

Received 16 November 2012

Revised 13 December 2012

Accepted 20 December 2012

Available online 9 January 2013

Keywords:

Protein–protein interaction inhibitors

Urokinase receptor

Metastasis

Breast cancer

Cancer

Virtual screening

Synthesis

In vivo

ABSTRACT

The uPAR·uPA protein–protein interaction (PPI) is involved in signaling and proteolytic events that promote tumor invasion and metastasis. A previous study had identified **4** (IPR-803) from computational screening of a commercial chemical library and shown that the compound inhibited uPAR·uPA PPI in competition biochemical assays and invasion cellular studies. Here, we synthesize **4** to evaluate in vivo pharmacokinetic (PK) and efficacy studies in a murine breast cancer metastasis model. First, we show, using fluorescence polarization and saturation transfer difference (STD) NMR, that **4** binds directly to uPAR with sub-micromolar affinity of 0.2 μM . We show that **4** blocks invasion of breast MDA-MB-231, and inhibits matrix metalloproteinase (MMP) breakdown of the extracellular matrix (ECM). Derivatives of **4** also inhibited MMP activity and blocked invasion in a concentration-dependent manner. Compound **4** also impaired MDA-MB-231 cell adhesion and migration. Extensive in vivo PK studies in NOD-SCID mice revealed a half-life of nearly 5 h and peak concentration of 5 μM . Similar levels of the inhibitor were detected in tumor tissue up to 10 h. Female NSG mice inoculated with highly malignant TMD-MDA-MB-231 in their mammary fat pads showed that **4** impaired metastasis to the lungs with only four of the treated mice showing severe or marked metastasis compared to ten for the untreated mice. Compound **4** is a promising template for the development of compounds with enhanced PK parameters and greater efficacy.

© 2013 Elsevier Ltd. All rights reserved.

Abbreviations: uPAR, urokinase receptor; uPA, urokinase-type plasminogen activator; suPAR, soluble urokinase receptor; uPA_{ATF}, amino terminal fragment of uPA; MMP, matrix metalloproteinase; FP, fluorescence polarization; NOD/SCID, non-obese diabetic severe combined immunodeficient; PK, pharmacokinetic; MDA-MB-231, MD Anderson metastatic breast; FBS, fetal bovine serum; DMEM, Dulbecco's Modified Eagle Medium; SDS, sodium dodecyl sulfate; CBB, coomassie brilliant blue; BSA, bovine serum albumin; DEAE, diethylaminoethyl cellulose; FITC, fluorescein isothiocyanate; TBST, tris-buffered saline and tween 20; IB, immunoblot; NMR, nuclear magnetic resonance; DCM, dichloromethane; HRMS, high-resolution mass spectrometry; THF, tetrahydrofuran; PDB, protein databank; DMAP, 4-dimethylaminopyridine; DCC, N,N'-dicyclohexylcarbodiimide; FAM, 6-carboxyfluorescein; HPLC, high-performance liquid chromatography; GPI, glycosylphosphatidylinositol; MTT, 3-(4,5-dimethylthiazol-2-yl)-2,5-diphenyltetrazolium bromide; TMD-MDA-MB-231, tumor-derived MDA-MB-231; AUC, area under the curve; AUMC, area under the moment curve; LARC, laboratory animal resources center; IACUC, institutional animal care and use committee; HPLC, high-performance liquid chromatography; PPI, protein–protein interaction; FN, fibronectin.

* Corresponding author.

E-mail address: smeroueh@iupui.edu (S.O. Meroueh).

1. Introduction

Cancer is a set of over 100 diseases that share a number of characteristics. Hanahan and Weinberg proposed several essential events as hallmarks of cancer,¹ including the ability of malignant cells to invade tissue and spread to distal sites (metastasis). Studies have shown that protein interactions of the urokinase receptor (uPAR) are involved in the complex processes that promote invasion and metastasis. uPAR has been implicated in nearly every step of cancer metastasis including cell migration,^{2,3} adhesion,^{4,5} angiogenesis,^{6,7} and invasion.^{5,8–10} This has led to attempts to inhibit its protein interactions. Most efforts to date have been confined to the use of biologics consisting of either fusion proteins^{11–13} or peptides.^{14–17} Recently, we have reported the first small organic molecules that inhibit the protein interaction of uPAR with its highest affinity ligand, the urokinase-type plasminogen activator (uPA).¹⁸ **11** (IPR-456) was identified using structure-based computational screening.¹⁸ A derivative of **11**, namely **4** (IPR-803), emerged from a substructure search of commercial chemical libraries and showed higher potency in blocking breast cancer invasion in cellular studies. A structure–activity study provided valuable insight into the functional groups required to effectively inhibit the uPAR–uPA interaction.¹⁹ The effect of these compounds on lung cancer metastasis in cell culture-based studies was investigated in the same study. The results showed that **4** and other compounds impaired invasion, migration and adhesion in a panel of non-small cell lung cancer (NSCLC) cell lines.¹⁹

In an effort to develop uPAR antagonists with in vivo efficacy, we focus on breast cancer metastasis. We synthesize **4**, for the first time, and assess it in a breast-to-lung orthotopic model. Previously, competition studies of **4** using surface plasmon resonance (SPR) established that it inhibited uPA_{ATF} binding to uPAR.¹⁸ Here, we probe the direct binding of the compound to uPAR by performing binding studies using fluorescence polarization and saturation transfer difference (STD) NMR. These studies afforded, for the first time, an equilibrium constant for binding to uPAR. Prior to performing in vivo studies, the effects of **4** on breast MDA-MB-231 invasion, migration and adhesion were explored. Extensive pharmacokinetic (PK) studies were carried out in SCID mice to generate PK parameters and measure the levels of the compound in plasma and tumor tissue. Finally, NSG mice were implanted with TMD-MDA-MB-231 (TMD-231) breast cancer cells in the mammary fat pads and dosed with **4** on a daily basis to assess its effect on breast cancer metastasis to the lungs.

2. Materials and methods

2.1. Fluorescence polarization

Varying concentrations of suPAR277 protein were titrated against intrinsically fluorescent **4** at a final concentration of 1 μ M in 1 \times PBS with 0.01% Triton X-100. The inhibitor–protein solution was incubated for 15 min. at room temperature. Polarized fluorescence intensities were measured using EnVision[®] Multilabel Plate Readers (PerkinElmer, Waltham, MA) with excitation and emission wavelengths of 531 and 595 nm, respectively.

2.2. STD NMR

To further characterize and confirm the binding of **4** to uPAR, saturation transfer difference (STD) nuclear magnetic resonance (NMR) was used.²⁰ Selective pulses were applied at 0.8 ppm to irradiate the protein methyl groups (where no ligand peaks appear) while the off-resonance frequency was positioned at 30 ppm. Saturation was carried out with a total 2 s pulse train

composed of a repeated 50 ms gauss shaped pulse and 0.1 ms inter-pulse delay. The STD experiment of the small-molecule with protein was acquired with 4096 scans. The same experiment was collected on small-molecule alone using exactly the same acquisition parameters except with 1024 scans. To ensure that we only observed magnetization from the small-molecule, the protein (uPAR) was added at a concentration of 50–100 fold less than the small-molecule. Compound **4** was dissolved in deuterated DMSO at a concentration of 50 mM; it was then diluted in phosphate buffer at a concentration of 0.7 mM for the NMR experiment. The compound was not fully soluble at 0.7 mM and thus the ratio of small-molecule to protein may not be exactly 50 fold. NMR experiments were acquired at 298 K on a VNMRs 800 MHz NMR spectrometer operating at a magnetic field strength of 18.8 T and equipped with a cold probe (Agilent Technologies, Santa Clara CA). Shigemi NMR tubes were used for the NMR experiments. Water suppression was done using Varian water sculpting pulse sequence.

2.3. Cell culture

MDA-MB-231 and TMD-231 were cultured in Dulbecco's Modified Eagle Medium (Cellgro, Manassas, VA) supplemented with 10% FBS and 1% penicillin/streptomycin in 5% CO₂ atmosphere at 37 °C.

2.4. Reagents

Biotinylated anti-human uPAR antibody (BAF807) was purchased from R&D Systems (Minneapolis, MN). Rabbit anti-human uPA antibody 389 was purchased from American Diagnostica Inc. (Stamford, CT).

2.5. Western blot analysis for MAPK signaling

Six well plates were coated with 30 ng μ L⁻¹ of fibronectin at 4 °C overnight. 1.5 \times 10⁶ serum starved MDA-MB-231 cells were plated onto each well in the presence of 1% DMSO (control) or 50 μ M of **4** or IPR-69, a previously described positive control for 30 min as previously described.¹⁹ Total cell lysates were prepared in standard RIPA extraction buffer containing protease and phosphatase inhibitors (Sigma). Thirty microgram of protein was separated by 10% SDS–PAGE and transferred to nitrocellulose membrane (Amersham, Arlington Heights, IL) and then blocked for 1 h at room temperature in PBS–1% fish gelatin buffer. The membrane was immunoprobed with phospho-p44/42 MAPK (Thr202/Tyr204) rabbit monoclonal antibody (1:2000) and p44/42 MAPK mouse monoclonal antibody (1:2000) at 4 °C overnight. Then, the membrane was incubated with IRDye 800-conjugated goat anti-mouse IgG (Rockland) and Alexa Fluor 680 goat anti-rabbit IgG (Invitrogen) as secondary antibodies (1:10,000). Bands were detected using Li-Cor Odyssey Imaging System (Li-Cor, Lincoln, NE).

2.6. Immunofluorescence imaging

MDA-MB-231 cells were grown on laminin- and poly-d-lysine-coated glass coverslips, exposed to 100 μ M of **4** or 100 μ M of **11** for 30 min at 37 °C, washed with PBS, fixed with 4% paraformaldehyde in PBS for 20 min, and permeabilized with 1% Triton X-100 in PBS for 10 min. Non-specific binding was blocked with 5% normal goat serum, 5% BSA, 0.01% Triton X-100 in PBS at RT for 1 h. The cells were incubated overnight at 4 °C with rabbit polyclonal antihuman uPA antibody 389 (dilution of 1:50 in 1% BSA/PBS). After 3-fold washing with PBS, the cells were incubated with anti-rabbit IgG conjugated with Alexa 594 Texas Red (Invitrogen Grand Island, NY), at a dilution of 1:500 in 1% BSA/PBS at RT for 1 h in the dark.

Images were acquired using a Nikon swept-field confocal microscope.

2.7. Invasion assay

Invasion transwell chambers were purchased from BD biosciences (San Jose, CA).²¹ The undersurface of the inserts was coated with 30 ng μL^{-1} of fibronectin at 4 °C overnight. The filters were equilibrated with 0.5 mL of serum-free medium for 2 h at 37 °C. After 4 h of serum starvation, cells were harvested and 5×10^4 cells in 500 μL medium containing 0.1% FBS and the indicated compounds or 1% DMSO control were plated onto the upper chamber of a transwell filter. Five hundred microlitre of 10% FBS medium containing the same amount of compounds or DMSO control was added to the lower chamber. After a 16 h incubation at 37 °C in 5% CO_2 , the filters were fixed and the number of cells that had invaded was determined as described below in the migration assay.

2.8. Transwell migration assay

24-well transwell plates (Costar, Corning, NY) were coated with 30 ng μL^{-1} of fibronectin at 4 °C overnight for migration assays as described previously.^{18,19} After 4 h of serum starvation, 5×10^4 cells in 250 μL of 0.1% FBS medium containing the indicated compounds or 1% DMSO control were added to the upper chamber and incubated at 37 °C for 16 h. 500 μL of 10% FBS medium containing the same amount of compounds or 1% DMSO control was simultaneously added to the lower chamber. Non-migrated cells on the top of the transwell were scrapped off with a cotton swab, and the cells that migrated through the filter were fixed in methanol for 30 min at room temperature and stained with Hematoxylin Stain (Fisher Scientific) for 1 h at room temperature. The filters were washed with water 3 times. Filters were air-dried, and the number of migrated cells was counted in ten separate fields and averaged across two independent experiments with each concentration in triplicate.

2.9. Adhesion assay

96-well plates were coated with 15 ng μL^{-1} fibronectin (Sigma–Aldrich, St. Louis, Missouri) at 4 °C overnight, then blocked with 2% BSA in PBS for 1 h, as described previously.^{14,18,19,22,23} After starving with serum-free medium for 4 h, MDA-MB-231 cells (2.5×10^5 cells mL^{-1}) were trypsinized and suspended in 100 μL of 0.1% FBS DMEM medium with various concentrations of compounds or DMSO control at 37 °C for 90 min. Medium was then carefully suctioned out from each well. Each well was washed three times with PBS. The wells were washed, and the number of adherent cells was quantified by MTT assay at 570 and 630 nm. Results are representative of three independent experiments with each concentration in quadruplicate. Similar results were obtained following harvesting the cells with trypsin or 2 mM EDTA for the control compound IPR-69 (data not shown).

2.10. Cell viability assay

10^4 mL^{-1} MDA-MB-231 cells were plated overnight in 100 μL /well of 96 well plates. Cells were treated with DMSO (control) or compounds at different concentrations for 3 days. Viable cells were quantified by MTT assay at absorbance of 570 with 630 nm for reference background as previously described.¹⁹

2.11. Gelatin zymography

MDA-MB-231 cells were treated with compounds in serum free medium for 24 h. The conditioned medium was collected and

concentrated by Amicon Ultra centrifugal filter units (Millipore, #UFC 501024), and proteins were normalized and electrophoresed on 7.5% sodium dodecyl sulfate (SDS) polyacrylamide gels containing 1 mg/mL gelatin. After electrophoresis, the gel was washed twice in 2.5% Triton X-100 for 30 min at room temperature and incubated in buffer that contained 50 mM Tris–HCl (pH 7.6), 200 mM NaCl, 10 mM CaCl_2 , and 0.02% Brij 35 at 37 °C for 36 h. Then, the gels were stained with 0.05% Coomassie brilliant blue (CBB) and de-stained with 30% methanol in 10% acetic acid. Areas of gelatinolytic degradation appeared as transparent bands on the blue stained background of the gel. Data were quantified using Li-Cor Odyssey Imaging System (Li-Cor, Lincoln, NE).

2.12. Cloning, expression and purification of uPAR

suPAR was obtained by a one-step purification process as previously described.²⁴

2.13. Western blot analysis

Total cell lysates were prepared in standard RIPA extraction buffer containing protease and phosphatase inhibitors (Sigma). Thirty μg of protein was separated by 10% SDS–PAGE and transferred to nitrocellulose membranes (Amersham, Arlington Heights, IL). The membranes were immunoprobed with uPAR (10G7), uPA (H-140) or Actin (C-2) antibodies (Santa Cruz Biotechnology, Santa Cruz, CA) at 4 °C overnight. Next, membranes were incubated with IRDye 800-conjugated goat anti-mouse IgG (Rockland) and Alexa Fluor 680 goat anti-rabbit IgG (Invitrogen) as secondary antibodies. Bands were detected using Li-Cor Odyssey Imaging System (Li-Cor, Lincoln, NE).

2.14. Apoptosis assay

MDA-MB-231 cells were treated with indicated concentrations of **4** or 1% DMSO control for 24 h and flow cytometry analysis was performed as described previously.¹⁹

2.15. Tissue preparation

All lung tissues were collected and fixed in 10% neutral buffered formalin within 30 min of removal during surgery. The tissues were fixed overnight in neutral buffered formalin and then transferred to 70 percent ethanol prior to processing to a paraffin block. The slides are then baked overnight at 59 °C in an oven before staining with H&E.

2.16. Slide evaluation

Three investigators examined the slides by light microscopy to examine for metastatic carcinoma in the lungs. Each lung lobe was analyzed for tumor cells and large tumor metastases. The number of lung metastases were counted in each lobe, and the size of the tumor foci were scored on a scale of 0 to 3+ (0, no staining; 1, mild: tumor foci composed of cells from 2 to 25; 2, moderate: tumor foci composed of cells from 25 to 150; 3, severe tumor foci composed of cells from 150 to 600 cells, and 4, marked: large coalescing tumor foci with 600 plus tumor cells). Each lobe was counted in its entirety.

2.17. Synthesis

All chemicals were purchased from commercially available sources and used as received. Column chromatography was carried out with silica gel (25–63 μ). High-Res Mass Spectra were measured on an Agilent 6520 Accurate Mass Q-TOF instrument. ¹H

NMR was recorded in CDCl_3 or DMSO on a Bruker 500 MHz spectrometer. RP-LCMS was carried out on a Agilent 1100 LC/MSD fitted with an Eclipse XBD-C18 (4.6×150 mm) column eluting at 1.0 ml/min employing a gradient of (acetonitrile:methanol):water (each containing 5 mM NH_4OAc) from 70% to 100% acetonitrile:methanol over 15 min and holding at 100% acetonitrile:methanol for 2 min. Chemical shifts are reported in ppm using either residual CHCl_3 or DMSO as internal references. Unless otherwise stated, the following procedures were modified or adopted from the literature.

2.18. 3,5-Dibromo-6H-anthra[1,9-cd]isoxazol-6-one (1)

Sodium nitrite (993 mg, 14.4 mmol) was added with stirring to concd H_2SO_4 (25 mL) at 30–40 °C over 10 min then stirred for an additional 30 min. Next 1-amino-2,4-dibromoanthraquinone (5.0 g, 13.1 mmol) was added over 15 min and the mixture was stirred overnight (16 h) at 50–55 °C. The heated solution was poured directly over ice and the resulting yellow precipitate was filtered, washed with cold water, and a 1:1 mixture of ethanol-ether. The moist anthraquinonediazonium hydrogensulfate was added to a solution of NaN_3 (1.37 g, 21.0 mmol) in water (25 mL) and stirred overnight (16 h). The light orange solid was filtered off and washed with water followed by a 9:1 mixture of acetone-water. The moist azide was suspended in toluene (40 mL) and heated to 70 °C with stirring. Water and acetone were slowly distilled (using a Dean–Stark apparatus) over a 12 h period. The yellow-orange crystals were filtered and washed with methanol to give 3.78 g (76%) of 3,5-dibromo-6H-anthra[1,9-cd]isoxazol-6-one.²⁵ ^1H NMR (500 MHz, CDCl_3) δ 8.44 (d, $J = 7.8$ Hz, 1H-C5), 8.07 (d, $J = 7.4$ Hz, 1H-C8), 7.97 (s, 1H), 7.80 (t, $J = 7.0$ Hz, 1H-C7), 7.71 (t, $J = 7.4$ Hz, 1H-C6); ^{13}C NMR (126 MHz, CDCl_3) δ 179.9, 153.6, 141.8, 134.0, 131.9, 131.4, 130.2, 125.0, 123.5, 123.5, 122.8, 121.6, 115.6. HRMS Calcd for $\text{C}_{14}\text{H}_5\text{Br}_2\text{NO}_2$ ($\text{M}+\text{H}^+$)⁺ 379.8742, found 379.8740.

2.19. Methyl 3-((3-bromo-6-oxo-6H-anthra[1,9-cd]isoxazol-5-yl)amino)benzoate (2)

To a solution of methyl 3-aminobenzoate (481 mg, 3.18 mmol) in nitrobenzene (3 mL), anhydrous AlCl_3 (353 mg, 2.65 mmol) was added with vigorous stirring. After 5 min, **1** was added and the reaction mixture stirred for 3 h at ambient temperature. The reaction mixture was poured into an ice-water slurry that precipitated a reddish solid which was filtered off. The reddish solid was recrystallized from toluene to give 144 mg (61%) of **2**.²⁶ ^1H NMR (500 MHz, CDCl_3) δ 11.40 (s, 1H-NH), 8.55 (d, $J = 8$ Hz, 1H-C5), 8.15 (d, $J = 8$ Hz, 1H-C8), 8.07–8.01 (m, 2H), 7.81 (t, $J = 7.5$ Hz, 1H-C7), 7.72–7.66 (m, 2H), 7.63–7.53 (m, 2H), 3.97 (s, 3H-OMe). ^{13}C NMR (126 MHz, CDCl_3) δ 181.0, 166.0, 157.9, 151.2, 148.7, 137.5, 132.7, 132.5, 132.2, 130.2, 129.3, 128.7, 128.6, 128.0, 126.5, 125.4, 123.5, 122.5, 119.9, 117.1, 101.9, 52.5. HRMS Calcd for $\text{C}_{22}\text{H}_{13}\text{BrN}_2\text{O}_4$ ($\text{M}+\text{H}^+$)⁺ 449.0135, found 449.0141.

2.20. Methyl 3-((3-(azepan-1-yl)-6-oxo-6H-anthra[1,9-cd]isoxazol-5-yl)amino)benzoate (3)

Hexamethylenimine (62 μL , 0.55 mmol) and **2** (100 mg, 0.22 mmol) were dissolved in acetonitrile (4 mL). The reaction solution was heated to 70–80 °C. As determined by TLC the reaction was complete after 3 h afterwards the reaction mixture was cooled to ambient temperature then to –15 °C for 1 h. The reddish solid was filtered off and washed with cold acetonitrile to give 52 mg (50%) of **3**.²⁷ ^1H NMR (500 MHz, CDCl_3) δ 11.94 (s, 1H-NH), 8.63 (d, $J = 8$ Hz, 1H-C5), 8.19–8.14 (m, 2H), 7.91 (d, $J = 7$ Hz, 1H, H para to amino group), 7.73 (t, $J = 7$ Hz, 1H-C7), 7.64 (t,

$J = 8$ Hz, 1H-C6), 7.58–7.50 (m, 2H), 6.18 (s, 1H), 4.51–3.40 (vbr s, 4H), 3.94 (s, 3H-OMe), 1.91 (br s, 4H), 1.65 (br s, 4H). ^{13}C NMR (126 MHz, CDCl_3) δ 176.0, 166.3, 154.7, 153.6, 148.0, 146.7, 139.1, 133.5, 131.4, 130.6, 129.7, 127.9, 127.7, 126.2, 124.2, 121.8, 118.9, 96.2, 91.9, 52.3, 26.6, 18.9. HRMS Calcd for $\text{C}_{28}\text{H}_{25}\text{N}_3\text{O}_4$ ($\text{M}-\text{H}$)⁻ 466.1775, found 466.1772.

2.21. 3-((3-(Azepan-1-yl)-6-oxo-6H-anthra[1,9-cd]isoxazol-5-yl)amino)benzoic acid (4)

Compound **3** (433 mg, 0.93 mmol) was hydrolyzed in a methanol (4 mL) and 2 M aq NaOH (2 mL) solution at 80 °C with stirring overnight. The residual methanol was removed in vacuo, and the resulting residue was acidified to pH 2. The precipitate was filtered off and washed with cold water to give **4** (314 mg, 74%) as a reddish-brown solid. ^1H NMR (500 MHz, DMSO) δ 11.79 (s, 1H-NH), 8.44 (app d, $J = 8$ Hz, 1H-C5), 8.13 (app d, $J = 8$ Hz, 1H-C8), 8.01 (s, 1H), 7.84–7.78 (m, 2H), 7.72–7.67 (m, 2H), 7.64–7.59 (m, 1H), 6.12 (s, 1H), 4.51–3.97 (br s, 4H), 1.80 (br s, 4H), 1.55 (br s, 4H); ^{13}C NMR (126 MHz, DMSO) δ 174.7, 166.8, 153.6, 152.8, 147.6, 146.0, 138.5, 132.9, 132.4, 131.2, 130.2, 128.3, 127.5, 127.4, 126.0, 123.4, 121.8, 118.5, 99.5, 95.0, 91.7, 56.0, 26.0, 18.6. HRMS Calcd for $\text{C}_{27}\text{H}_{22}\text{N}_3\text{O}_4$ ($\text{M}-\text{H}$)⁻ 452.1610, found 452.1601.

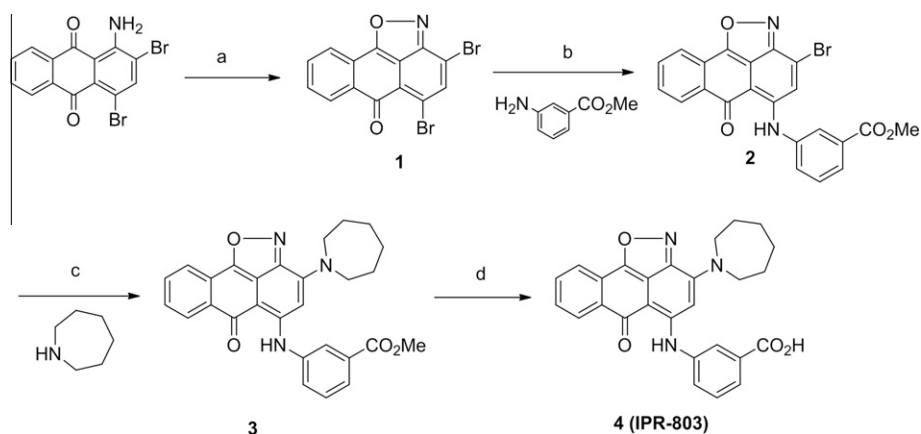
3. Results

3.1. Synthesis of 4

Despite its availability in a commercial database, the synthesis of **4** has not been reported. To enable cellular and in vivo studies of the compound, we conceived a synthesis route that successfully led to the preparation of the compound in gram-scale (Scheme 1). It consisted of first preparing 3,5-dibromo-6H-anthra[1,9-cd]isoxazol-6-one by the diazotation of 1-amino-2,4-dibromoanthraquinone. This was accomplished by adding sodium nitrite to a solution of the amine in concentrated sulfuric acid to give the 1-anthraquinonediazonium hydrogen sulfate, which was subsequently converted to the 1-azidoanthraquinone by reacting with an aqueous solution of sodium azide. The azidoanthraquinone was azeotropically refluxed in toluene to provide, by evolution of nitrogen, the required isoxazole ring in **1**.²⁵ Arylamination of **1** at the 5-position was accomplished with anhydrous AlCl_3 in nitrobenzene at ambient temperature to give a moderate yield of the 6-arylamino substituted.²⁶ This occurs by an increase in electrophilicity at the 4-bromo position via conjugation with the keto group after its complexation with AlCl_3 . A second amination was carried out at the 3-position using refluxing acetonitrile to give a moderate yield of **3**.²⁷ Next, hydrolysis of the benzoate ester **3** to the carboxylic acid **4** occurred under conditions of heating an aqueous solution of sodium hydroxide and methanol.

3.2. Direct binding and inhibition studies

In a previous study, we had reported the use of SPR to show that **4** inhibited uPA binding to uPAR in a concentration-dependent manner.¹⁸ Here, we sought to provide evidence that **4** inhibited the protein interaction by direct binding to uPAR. We also use this opportunity to determine a binding constant for the compound. The red-shifted fluorescence of **4** was exploited to measure its direct binding to uPAR using fluorescence polarization (FP).¹⁸ When exposed to a larger binding partner, a small-molecule is expected to adopt a slower tumbling rate leading to an increase in light polarization. Increasing the concentration of uPAR in the presence of **4** at a fixed concentration of 1 μM led to a corresponding increase in fluorescence polarization (Fig. 1A). This confirmed the



Scheme 1. Reagents and conditions: (a) $\text{NaNO}_2/\text{H}_2\text{SO}_4$, NaN_3 , toluene, reflux; (b) AlCl_3 , nitrobenzene, rt; (c) acetonitrile, 80°C ; (d) aq NaOH/MeOH 80°C .

direct binding of **4** to uPAR. A fit of the data resulted in a dissociation constant K_D of $0.19\ \mu\text{M}$. When the titration of **4** with uPAR was repeated in the presence of excess uPA_{ATF} at $50\ \mu\text{M}$ concentration, no increase in FP was detected (Fig. 1A). This suggests that **4** and uPA_{ATF} compete for the same site on the receptor.

To further confirm the binding of **4** to uPAR and gain additional insight into the recognition process, we resorted to the use of saturation transfer difference (STD) NMR. STD NMR is an entirely ligand-based method, such that measurement of the binding of a small-molecule to a protein is done by monitoring the transfer of magnetization by fast chemical exchange. First, a standard 1D spectrum of **4** was collected alone (Fig. 1B) and in the presence of uPAR (Fig. 1C). Comparison of the two spectra reveals that two NH peaks for the compound alone (inset of Fig. 1B). These peaks disappear when uPAR is added (inset of Fig. 1C). This observation

is evidence that **4** binds to uPAR. STD spectra for **4** alone (Fig. 1D) and in the presence of uPAR (Fig. 1E) were subsequently collected. In the presence of uPAR, there are distinctive peaks that are attributed to **4** (Fig. 1E). These peaks occur only when spin diffusion signal (originating from the protein) is transferred to the small-molecule. This indicates that the small-molecule is binding. In addition, comparison of Figure 1D and E shows distinct peaks for **4**, further confirming binding of the compound to uPAR.

3.3. Effect of **4** on uPAR-uPA binding in cells

Immunofluorescence confocal microscopy was used to probe the effect of **4** on the uPAR-uPA interaction at the cell surface of breast MDA-MB-231 cancer cells. Endogenous uPA in a breast cancer cell line MDA-MB-231 was immunostained with a selective

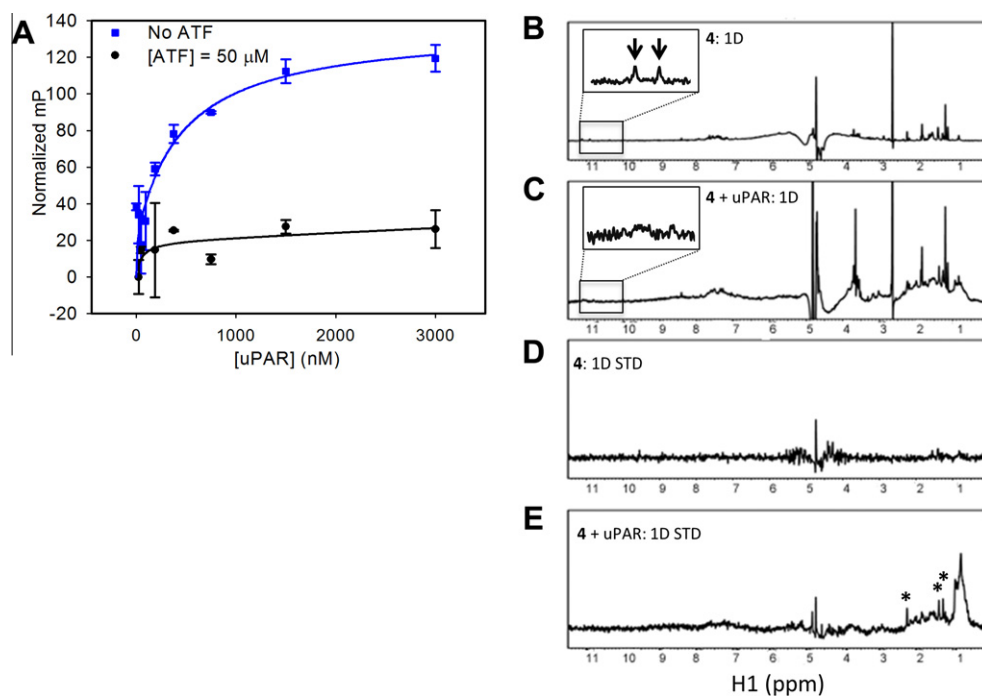


Figure 1. Biochemical characterization of **4**: (A) Direct binding of **4** to uPAR probed with fluorescence polarization with increasing concentration of uPAR; (B–E) STD NMR experiments were used to probe direct binding of **4** to uPAR; (B) 1D NMR spectrum of **4** only, the NH peaks of **4** highlighted by arrows in the inset, which shows region inside the box magnified, are broadened in the presence of uPAR as shown in the inset of the spectrum below; (C) 1D NMR spectrum of **4** in the presence of uPAR; (D) STD NMR spectrum of **4** only showing no ligand peaks arising; (E) STD NMR spectrum of **4** in the presence of uPAR where peaks highlighted with asterisks represent peaks arising from binding of **4** to uPAR. Saturation of the protein peaks was set at 0.8 ppm.

antibody and subsequently visualized by staining with a fluorescently conjugated secondary antibody. Representative deconvolved confocal immunofluorescence images are presented in Figure 2A and B. To get a quantitative estimate of the effect of **4** on the uPA level, we quantified its surface staining intensity (Fig. 2C). The pixel immunodensities for uPA were determined using Nikon elements software. In the absence of any compound (DMSO; vehicle control), uPA was detected in intracellular clusters as well as on surface membranes of the MDA-MB-231 cells (Fig. 2A, arrows). In the presence of **4**, added 30 min prior to immunostaining, there was a significant reduction of uPA staining at the cell surface (Fig. 2C). Surface staining was reduced by ~95% and ~80% at 100 μ M of **4** and at 100 μ M of **11**, respectively. These results suggest that **4** can effectively prevent uPA from binding to uPAR, supporting the findings from our biochemical assays that **4** acts as a direct inhibitor of the PPI.

3.4. Effect of **4** on invasion, migration and adhesion of MDA-MB-231 cells

Previously, we had shown that siRNA knockdown of uPAR in MDA-MB-231 cells resulted in more than 60 percent impairment of cell invasion.¹⁸ We had also shown that **4**, which was purchased from a commercial library, inhibited MDA-MB-231 invasion using the same Boyden chamber apparatus. Here, we confirm that our

synthesized compound showed similar inhibition of invasion as the purchased compound reported earlier (Fig. S1).¹⁸ To gain further insight into the mechanism by which these compounds inhibit invasion, we study the effect of the compound on matrix metalloproteinase (MMP) activity using gelatin zymography. MMPs are well-known proteases that degrade components of the ECM, such as collagen, laminin, fibronectin and vitronectin. Activation of MMPs is promoted by uPA binding to uPAR. We found that **4** effectively inhibited matrix metalloproteinase (MMP-9) mediated degradation of gelatin in a concentration-dependent manner (Fig. 3A). At 25 μ M nearly 40 percent inhibition is achieved. Cell viability studies using MTT were carried out on **4** to evaluate its effects on MDA-MB-231 cell growth. A concentration-dependent curve was constructed over a period of 3 days. It resulted in an IC_{50} of 58 μ M for **4** (Fig. 3B). Since the invasion studies are carried out over a significantly shorter time, and given the more than 90 percent blockage of invasion that is observed for **4** at 50 μ M, it is therefore expected that most of the inhibition of cell invasion is unlikely due to cytotoxicity of the compound.

For cells to effectively metastasize, they must acquire additional phenotypes, such as adhesion and migration. The Boyden chamber apparatus without the Matrigel layer can be used to assess the effect of **4** on cell migration (Fig. 3C). At 40 μ M, nearly 30 percent inhibition of MDA-MB-231 migration is observed, and at 80 μ M nearly 70 percent inhibition is measured. The effect of **4** on

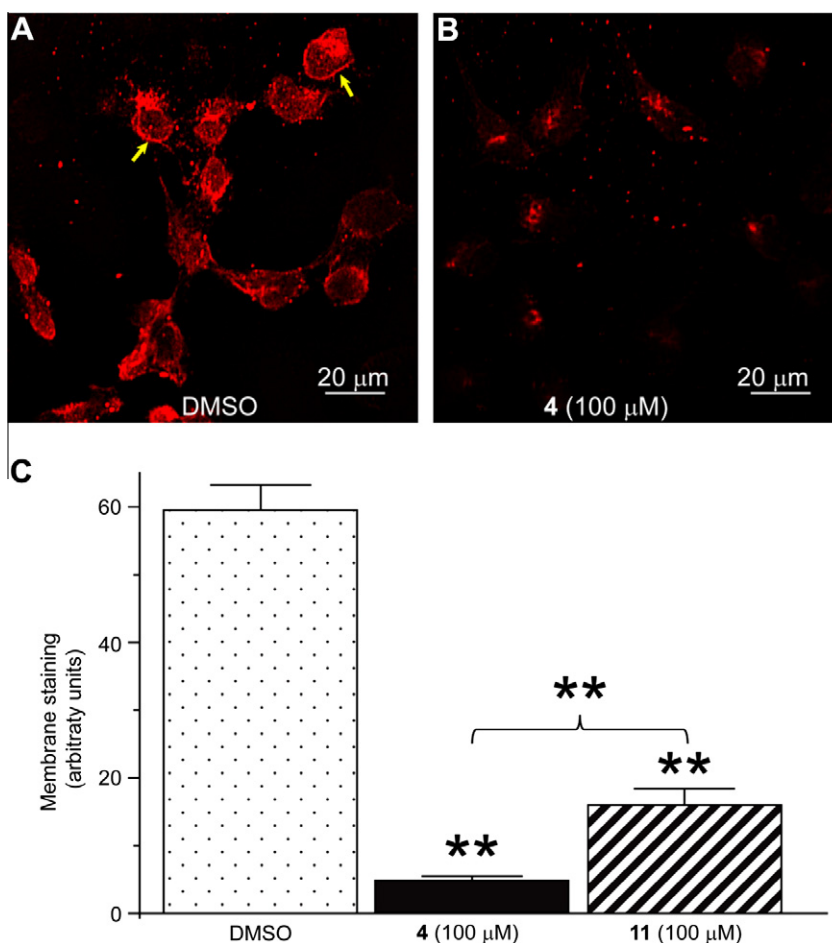


Figure 2. Immunofluorescence imaging to probe inhibition in cells: Representative deconvolved confocal immunofluorescence images of MDA-MB-231 cells incubated with DMSO (control, A) or 100 μ M of **4** (B) and visualized by staining with a polyclonal antibody against uPA (red). Arrows indicate examples of two cells with clear surface staining of uPA; (C) quantification of the surface expression levels of uPA in MDA-MB-231 cells exposed to the indicated conditions. 100 μ M of the previously reported **11** was used as a positive control.^{18,19} The pixel immunodensity of the surface uPA compared to the total staining of uPA was calculated. Only cells where the cell membrane was clearly discernible were included in the analyses. Each value represents the mean \pm SE from 17 to 38 cells taken from six different fields from two independent samples.

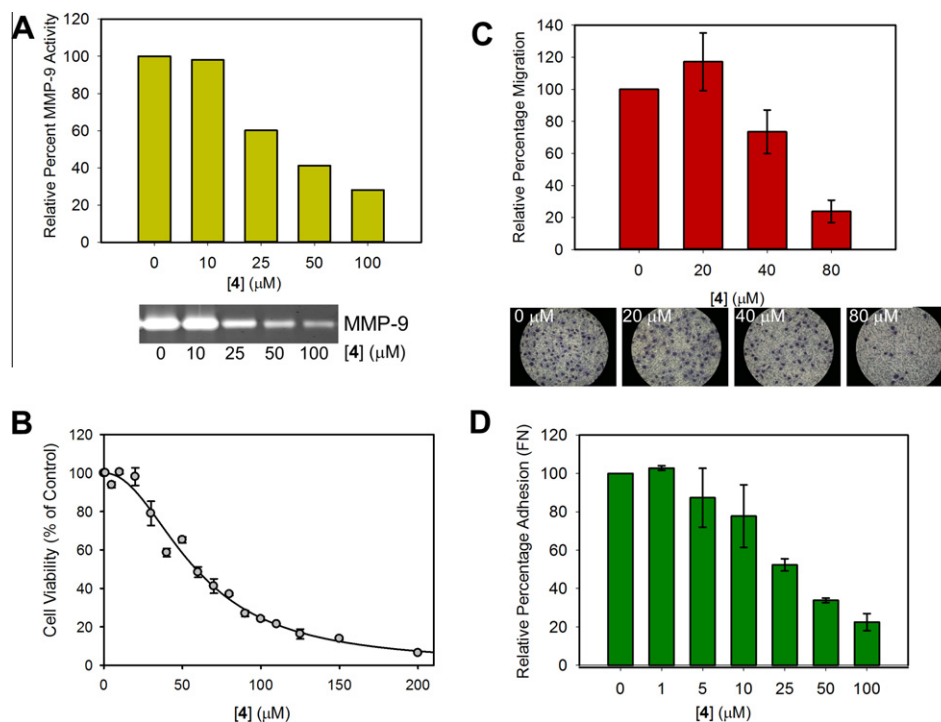


Figure 3. Invasion, migration and adhesion studies: (A) Matrix metalloproteinase (MMP-9) activity using gelatin zymography. Results are representative of three independent experiments; (B) effect of **4** on MDA-MB-231 cell viability as assessed by MTT assay; (C) cell migration studies with the Boyden chamber apparatus to characterize the role of **4** in chemotaxis-mediated cell migration; Error bars represent means \pm S.D. Representative experimental cells from control and in the presence of **4** were photographed ($\times 400$) to illustrate the effect of **4** on migration, as shown below; (D) effect of **4** on MDA-MB-231 cell attachment to fibronectin; error bars represent means \pm S.D.

adhesion was studied using MDA-MB-231 cells that were added to wells pre-coated with fibronectin as we have done previously.¹⁸ In the presence of **4**, a concentration-dependent impairment of cell adhesion is observed with an IC_{50} of approximately 30 μM (Fig. 3D). The effect on adhesion, albeit weaker than those observed in invasion, may be attributed to the effect of the compound on other interactions mediated by uPAR.

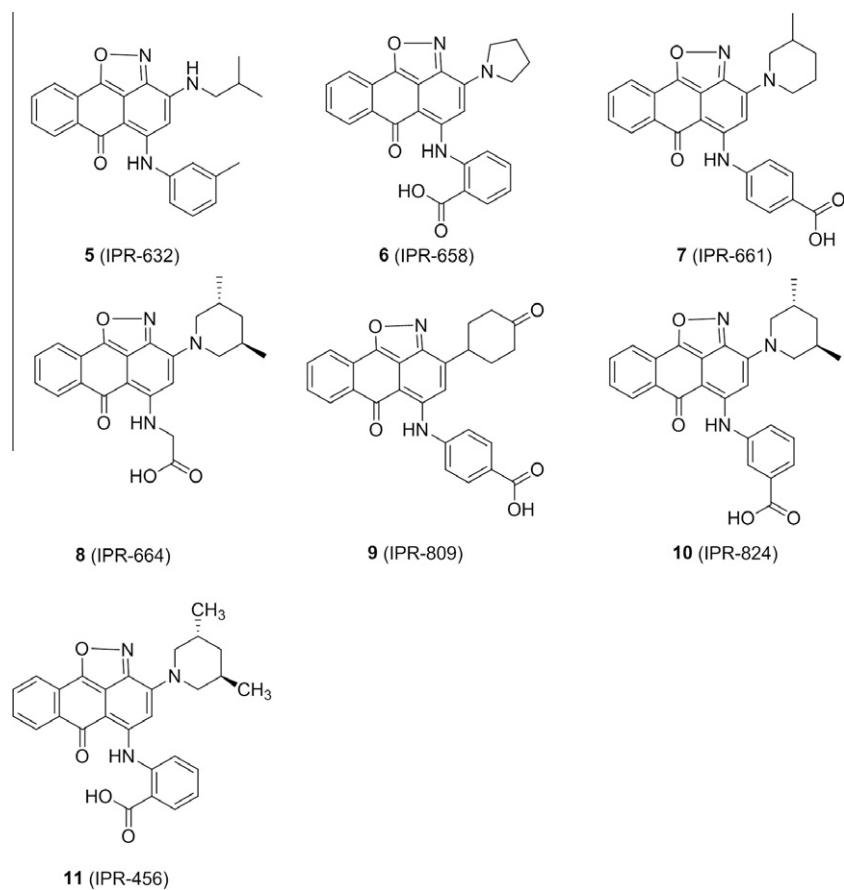
A limited structure–activity study is conducted on six derivatives of **4** (Scheme 2). Their effect on ECM degradation was determined with gelatin zymography (Fig. 4). The binding affinity of these compounds to uPAR was recently assessed in a comprehensive structure–activity (SAR) study.²⁸ A range of anti-invasion activity was observed for the compounds. At a concentration of 50 μM , **4** showed highest potency with nearly 90% inhibition of gelatinase activity. The compound was more active than the parent **11**, which showed about 40% inhibition. **5** (IPR-632) revealed no inhibition, consistent with findings from a previous study that the compound did not inhibit the tight uPAR–uPA interaction.²⁸ **6** (IPR-658) and **8** (IPR-664) inhibit the uPAR–uPA more weakly,²⁸ consistent with their reduced efficacy in blocking ECM degradation (Fig. 4). Compound **10** (IPR-824) is more potent than **7** (IPR-661) consistent with our previous observation that *m*-carboxylate is more effective than *p*-carboxylate in blocking binding of uPA to uPAR. Compound **9** (IPR-809) also inhibited gelatinase activity despite its significantly weaker inhibition of uPAR–uPA.²⁸ We had previously argued that the combination of a *para*-carboxylate on the benzoic acid moiety with a piperidinone may have contributed to its weaker activity and potential off-target effects. Invasion studies using the Boyden chamber apparatus confirmed the gelatin zymography results. For example, compound **7** inhibited MDA-MB-231 cell invasion in a concentration-dependent manner with an IC_{50} of approximately 30 μM (Fig. S2A). Cell viability studies using MTT over a period of three days revealed an IC_{50} of 33 μM for **7** (Fig. S2B).

To determine whether **4** cause apoptosis, a flow cytometry analysis was performed with Annexin V–FITC and PI staining. The level of apoptosis and necrosis in MDA-MB-231 cells was assessed after exposure to increasing concentrations of **4** for 24 h as a percentage of Annexin V–positive/PI–negative cells (apoptotic) and Annexin V–positive/PI–positive cells (necrotic) respectively (Fig. S3). Control DMSO treated cells showed 3 percent apoptotic and 6 percent necrotic cells (Fig. S3A). At concentrations of 1 (Fig. S3B), 10 (Fig. S3C), 25 (Fig. S3D) and 50 μM (Fig. S3E), **4** showed 3, 2, 2 and 0 percent apoptotic cells and 7, 5, 6 and 3 percent necrotic cells, respectively. These results indicate that **4** does not have a significant effect on apoptosis or necrosis.

We also tested the effects of **4** on MAPK signaling following plating of serum starved cells onto fibronectin-coated culture plates for 30 min in the presence of 1% DMSO control, 50 μM of **4** or 50 μM of IPR-69, a previously described compound that was used as a positive control. Western immunoblotting shows that as compared to DMSO control, IPR-69 significantly impaired MAPK phosphorylation as previously shown.¹⁹ **4** also showed inhibition of MAPK phosphorylation, as compared to DMSO control but the effect was weaker than that IPR-69 (Fig. S4).

3.5. In vivo PK studies

Compound **4** was administered to mice via a single PO delivery at 200 mg/kg using a formulation of saline. Blood (20 μL) was taken from the mice at their tails at 1, 2, 4, 6, 8 and 10 h (three time points from each of the 18 mice²⁹) post injection. Plasma was separated from blood and **4** was quantified by internal standardization, protein precipitation, and HPLC–MS/MS (Fig. 5A). The lower limit of quantification was 100 ng/mL using 20 μL of plasma. The compound was detected in plasma reaching a maximum concentration (C_{max}) of 5 μM after 1 h (t_{max}) (Fig. 5C). The stability of the compound in plasma is reflected by its half-life ($t_{1/2}$) that was estimated at 5 h. To gain



Scheme 2. Structure of derivatives of **4**.

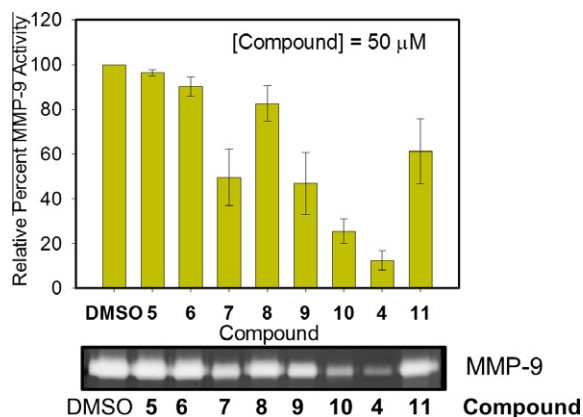


Figure 4. Invasion and cytotoxicity studies of **4** and its derivatives: Gelatin zymogram (below) showing the effects of **4** derivatives at 50 μM concentration on matrix metalloproteinase (MMP-9) activity as quantified above. Error bars represent means ± S.D.

insight into its absorption following oral dosing, intravenous bioavailability of **4** was determined. The compound was injected intravenously (IV) into the tail vein. Blood samples were obtained at 5, 10, 20, 45 and 120 min (three mice per time point) post injection. Plasma was separated from blood and **4** was quantified by internal standardization, protein precipitation, and HPLC–MS/MS (Fig. 5B). Based on these data, the oral bioavailability was 4 percent. Despite the low bioavailability in plasma, HPLC–MS/MS quantification of **4** in the primary tumor at 1, 4, and 10 h intervals detected the inhibitor at

concentrations near 10 μM. The levels of the compound in tumor tissue remained high even after 10 h.

3.6. Effect on breast cancer metastasis

An evaluation of the efficacy of **4** on metastasis was conducted in vivo using an orthotopic model that we have previously implemented.¹⁹ TMD-231 cells were inoculated into the mammary fat pads of female NSG mice. Like MDA-MB-231, TMD-231 overexpress uPAR as shown by immunoblotting analysis in Figure 6A. Dosing was initiated at day 15 post implantation. Animals were randomized and treated with vehicle or with **4** by daily oral gavage at a dose of 200 mg/kg ($n = 13$). Tumor volumes were determined by caliper measurements on a twice weekly basis, and calculated according to the formula $(\alpha^2 \times \beta)/2$, where α is the shorter and β is the longer of the two dimensions. The study was conducted over a period of 33 days. The primary tumor in both control and treated mice grew over the course of the study (Fig. 6B). Tumor volumes reached nearly 693 and 785 mm³ for treated and untreated mice, respectively. The small effect (~10%) on tumor size is fully consistent with previous studies that have shown that uPAR is not a lethal target. In addition, these studies further support our cellular studies that have found that **4** is not cytotoxic with IC₅₀ of 58 μM. There was no statistical significance to the differences in body weight between treated and untreated, suggesting that the compound may be well tolerated by the mice (Fig. 6C).

To assess the effect of **4** on metastasis, control and experimental animals were sacrificed and organs (lungs) were removed and evaluated for the presence of tumors. The analysis of tumor metastasis lesions showed that they ranged roughly from 2 to 25 cells, 25

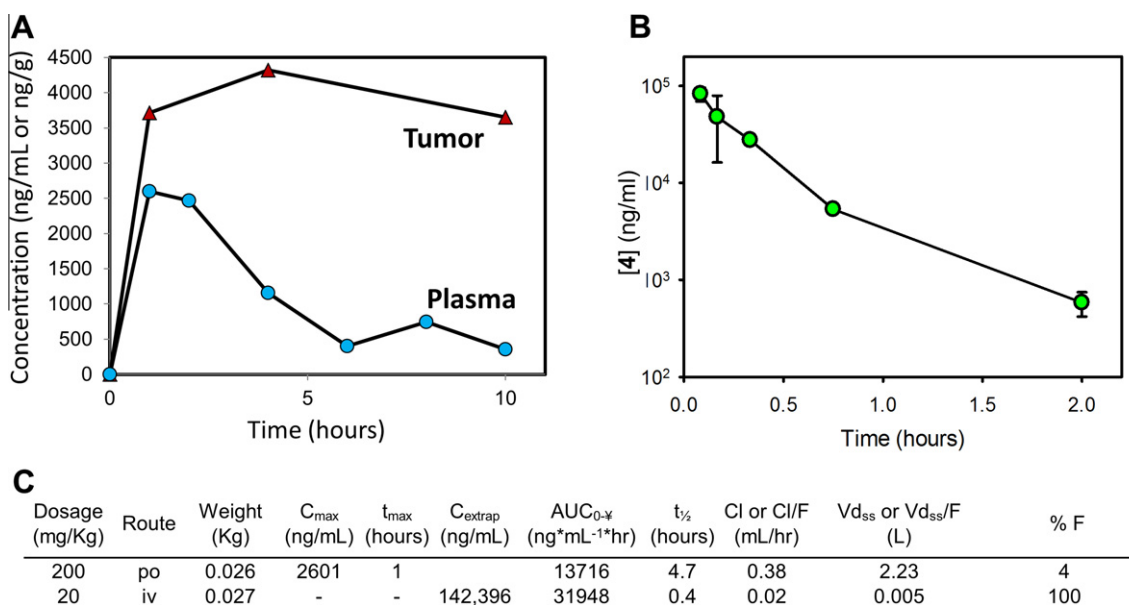


Figure 5. *In vivo* PK parameters: (A) PK analysis of **4** in female NOD/SCID mice ($n = 3$ per time point) dosed by oral gavage (200 mg/Kg); (B) plasma levels of **4** as a result of intravenous injection; (C) PK parameters.

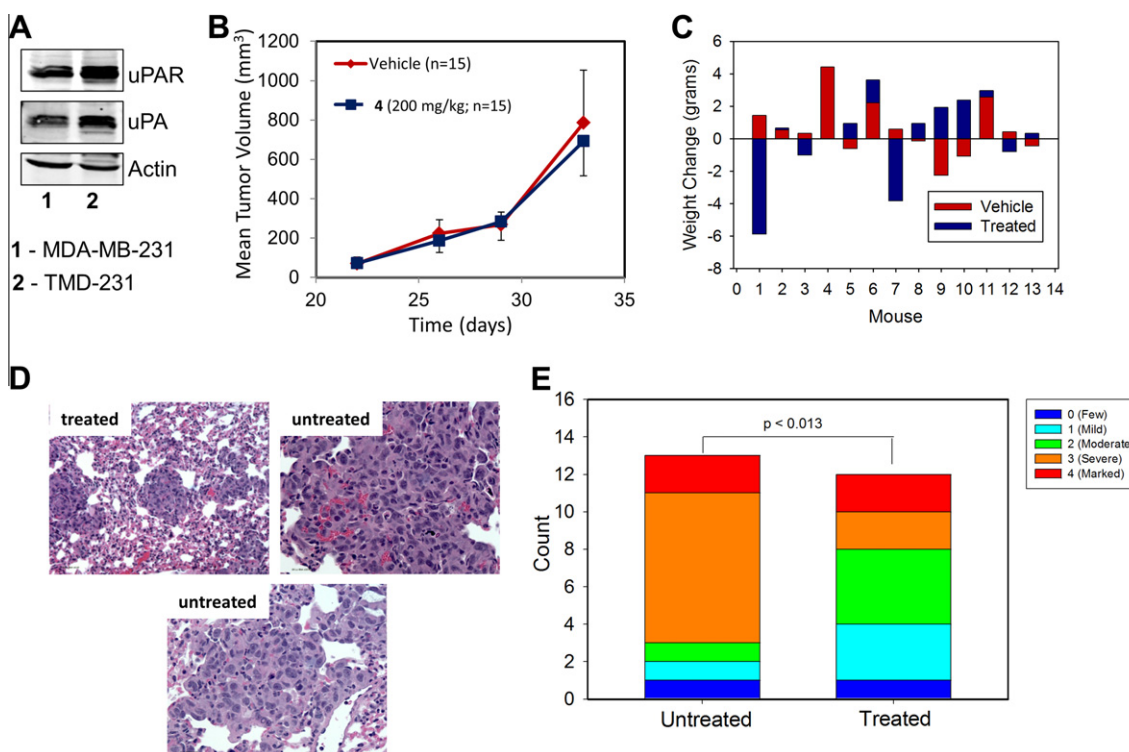


Figure 6. *In vivo* efficacy studies: (A) Western immunoblot showing the expression levels of uPAR and uPA in MDA-MB-231 and TMD-231 cell lines; (B) effect of **4** on TMD-231 tumor growth. TMD-231 cells were inoculated in the mammary fat pads of female NOD/SCID mice. Once the tumor volume reached 30–50 mm³, animals were randomized and treated with vehicle alone as control or 200 mg/kg of compound **4** three times a week for 5 weeks by oral gavage. Tumor volumes were determined by caliper measurements obtained weekly; (C) body weight change upon completion of the study after 33 days; (D) representative H&E staining images that illustrate metastasis in the lungs of animals; (E) scoring system was used to quantify the level of metastasis in the lungs. The number of lung tumor nuclei/cells were counted in each lobe, and their size were scored on a scale of 0–4 (0, few; 1, mild; 2, moderate; 3, severe; and 4: marked).

to 150 cells, and about 150 to 600 cells. There were a few large clusters of coalescing tumor balls seen. A few vehicle control lungs had tumor metastases that were coalescing into large tumor balls (greater than 1000 cells). The metastases were characterized by very large bizarre cells, which had large undifferentiated nuclei with large nucleoli. These were easy to discern by routine H&E staining and count. The number and size of metastasis in two to

five fields per sample were calculated. A score of 4+ was given to a sample with highest metastasis index and relative metastasis in other samples are calculated (i.e., 1+, 2+, 3+) by a sample-blinded pathologist (Fig. 6E). The extent of metastasis in treated versus untreated was significantly different. For example, 10 out of 13 untreated mice developed severe (score = 3) or marked (score = 4) metastasis to the lung. This is compared to only 4 out

of 12 in the treated mice (2 severe and 2 marked). Among the treated mice, 4 developed moderate (score = 2) metastasis. Another four were scored at 1 or lower, showing mild metastasis to the lungs. Representative H&E staining images for control and treated mice are shown in Figure 6D.

4. Discussion

Recently, we reported the discovery of **11**, a small-molecule inhibits the tight PPI between uPAR and its ligand uPA.¹⁸ A derivative, namely **4**, was also found to inhibit the PPI.²⁸ A recent study showed that **4** inhibited invasion in a panel of non-small cell lung cancer (NSCLC) cells.²⁸ Here, we extend on these studies and focus on probing uPAR with **4** in breast cancer metastasis and assess its efficacy in animal studies. The compound, which was previously purchased, is prepared in gram-scale to enable in vivo studies. In a departure from previous work that was confined to competition studies, direct binding studies are carried out using fluorescence polarization and STD NMR. These showed that the compound binds directly to uPAR with a sub-micromolar affinity of 0.2 μM , which is nearly an order of magnitude higher than previously-measured IC_{50} in competition assays. The nearly 10-fold difference between K_D and IC_{50} is not unexpected. The binding interface of the uPAR-uPA PPI (estimated at 1200 \AA^2) is significantly larger than the surface occupied by the small-molecule. Hence, a higher concentration of the compound is required to shift the equilibrium towards dissociation of the PPI complex. STD NMR studies not only provided further confirmation that the compounds binds to uPAR directly, but also generated data that supports the computationally predicted binding mode of **4**.

Compound **4** and its derivatives were used to probe the role of the uPAR-uPA interaction in breast cancer cell invasion and metastasis. Gelatin zymography revealed that MMP-9 activity is impaired by **4**, suggesting that blocking uPA binding to uPAR likely affects activation of uPA and the subsequent proteolytic cascade that has been shown to lead to MMP activation.^{30–32} The effects of **4** on cell adhesion ($\text{IC}_{50} = 30 \mu\text{M}$) and its weaker effect on migration ($\text{IC}_{50} = 50 \mu\text{M}$) may be attributed to inhibition of uPAR binding to integrins. It is well-known that uPAR engages integrins, which are responsible for attachment of cells to ECM components and migration.^{22,33,34} Although the integrin binding pocket is located away from the uPA binding site where **4** was targeted,³³ studies have shown cooperativity between uPA and vitronectin binding.³⁵ Extensive biophysical studies have shown that uPA binding to uPAR stabilizes the receptor and promotes binding to vitronectin.^{36,37} Hence, blocking of uPA binding by **4** likely alters the dynamics of uPAR resulting in impaired vitronectin binding and therefore less interaction with integrins. However, recent FRET-based cellular studies have shown that the uPAR-integrin interaction can occur even in the absence of uPA.³⁸ Since uPA is highly expressed in malignant cells, the effects on adhesion of our compounds could be attributed to destabilization of the uPAR-vitronectin complex. It is interesting that **4** inhibited signal transduction of the MAPK pathway, consistent with previous studies that have reported a role for uPAR in MAPK signaling.

The inhibition of the uPAR-uPA interaction and the effect of **4** on invasion prompted us to probe the compound for its effect on metastasis in vivo. When administered orally, **4** reached a concentration of 5 μM in plasma. It was encouraging that the levels of the compound in tumor tissue also reached a high concentration of up to 10 μM and was stable even after 10 h. The accumulation of the compound in tumor ensures constant binding to uPAR and inhibition of uPA binding. The half-life of the compound in plasma is estimated at nearly 5 h. The high levels of the compound in plasma and tumor tissue despite the low bioavailability of **4** percent

suggests that small improvements in absorption could result in significant increases in plasma and tumor concentrations.

In vivo, compound **4** was tested using an orthotopic breast-to-lung metastasis model that we had previously implemented.¹⁹ TMD-231 cells are highly aggressive breast cancer cell lines derived from MDA-MB-231.³⁹ Just like MDA-MB-231, TMD-231 cells overexpress uPAR. Analysis of the tumor growth reveals that **4** had little effect on tumor growth, in agreement with the weak cytotoxicity that was found in our proliferation assay study. The lack of cytotoxicity is consistent with the fact that uPAR is not required for normal biological function, as it is not even expressed in normal cells except during embryogenesis.^{40,41} It is highly expressed during inflammation^{42,43} or metastasis.^{44,45} The confined effect of **4** on metastasis and the lack of cytotoxicity suggest selectivity. Compound **4** and its analogs are the first small-molecules that have been identified to inhibit the uPAR-uPA PPI. These results are an excellent starting point, as **4** provides a lead molecule for the design and synthesis of derivatives with higher affinity and better PK properties.

Acknowledgments

The research was supported by the National Institutes of Health (CA135380) (SOM), the INGEN grant from the Lilly Endowment, Inc (SOM), by The Indiana University Melvin and Bren Simon Cancer Center Translational Research Acceleration Collaboration (ITRAC) (SOM), the Showalter Trust (SOM), by the Indiana University Biomedical Research Fund (SOM) and by the American Cancer Society Research Scholar Grant RSG-12-092-01-CDD (SOM). We acknowledge the analytical work performed by the Clinical Pharmacology Analytical Core laboratory, a core laboratory of the Indiana University Melvin and Bren Simon Cancer Center supported by the National Cancer Institute grant P30 CA082709.

Supplementary data

Supplementary data associated with this article can be found, in the online version, at <http://dx.doi.org/10.1016/j.bmc.2012.12.047>.

References and notes

- Hanahan, D.; Weinberg, R. A. *Cell* **2011**, *144*, 646.
- Prager, G. W.; Breuss, J. M.; Steurer, S.; Olcaydu, D.; Mihaly, J.; Brunner, P. M.; Stockinger, H.; Binder, B. R. *Circ. Res.* **2004**, *94*, 1562.
- Schiller, H. B.; Szekeres, A.; Binder, B. R.; Stockinger, H.; Leksa, V. *Mol. Biol. Cell* **2009**, *20*, 745.
- Andreasen, P. A.; Kjoller, L.; Christensen, L.; Duffy, M. J. *Int. J. Cancer* **1997**, *72*, 1.
- Liang, X.; Yang, X.; Tang, Y.; Zhou, H.; Liu, X.; Xiao, L.; et al. *Oral. Oncol.* **2008**, *44*, 1172.
- Mignatti, P.; Rifkin, D. B. *Enzyme Protein* **1996**, *49*, 117.
- Rabhani, S. A.; Mazar, A. P. *Surg. Oncol. Clin. North Am.* **2001**, *10*, 393.
- Kondraganti, S.; Gondi, C. S.; McCutcheon, I.; Dinh, D. H.; Gujrati, M.; Rao, J. S.; Olivero, W. C. *Int. J. Oncol.* **2006**, *28*, 1353.
- Subramanian, R.; Gondi, C. S.; Lakka, S. S.; Jutla, A.; Rao, J. S. *Int. J. Oncol.* **2006**, *28*, 831.
- Kunigal, S.; Lakka, S. S.; Gondi, C. S.; Estes, N.; Rao, J. S. *Int. J. Cancer* **2007**, *121*, 2307.
- Crowley, C. W.; Cohen, R. L.; Lucas, B. K.; Liu, G. H.; Shuman, M. A.; Levinson, A. D. *Proc. Natl. Acad. Sci. U.S.A.* **1993**, *90*, 5021.
- Ignar, D. M.; Andrews, J. L.; Witherspoon, S. M.; Leray, J. D.; Clay, W. C.; Kilpatrick, K.; Onori, J.; Kost, T.; Emerson, D. L. *Clin. Exp. Metastasis* **1998**, *16*, 9.
- Kobayashi, H.; Sugino, D.; She, M. Y.; Ohi, H.; Hirashima, Y.; Shinohara, H.; Fujie, M.; Shibata, K.; Terao, T. *Eur. J. Biochem.* **1998**, *253*, 817.
- Wei, Y.; Lukashev, M.; Simon, D. I.; Bodary, S. C.; Rosenberg, S.; Doyle, M. V.; Chapman, H. A. *Science* **1996**, *273*, 1551.
- Wei, Y.; Eble, J. A.; Wang, Z. M.; Kreidberg, J. A.; Chapman, H. A. *Mol. Biol. Cell* **2001**, *12*, 2975.
- Berkenblit, A.; Matulonis, U. A.; Kroener, J. F.; Dezube, B. J.; Lam, G. N.; Cuasay, L. C.; Brunner, N.; Jones, T. R.; Silverman, M. H.; Gold, M. A. *Gynecol. Oncol.* **2005**, *99*, 50.
- Guo, Y.; Higazi, A. A.; Arakelian, A.; Sachais, B. S.; Cines, D.; Goldfarb, R. H.; Jones, T. R.; Kwaan, H.; Mazar, A. P.; Rabhani, S. A. *FASEB J.* **2000**, *14*, 1400.

18. Khanna, M.; Wang, F.; Jo, I.; Knabe, W. E.; Wilson, S. M.; Li, L.; Bum-Erdene, K.; Li, J.; Khanna, R.; Meroueh, S. O. *ACS Chem. Biol.* **2011**, *6*, 1232.
19. Wang, F.; Li, J.; Sinn, A. L.; Knabe, W. E.; Khanna, M.; Jo, I.; Silver, J. M.; Oh, K.; Li, L.; Sandusky, G. E.; Sledge, G. W.; Nakshatri, H.; Jones, D. R.; Pollok, K. E.; Meroueh, S. O. *J. Med. Chem.* **2011**, *54*, 7193.
20. Meyer, B.; Peters, T. *Angew. Chem., Int. Ed.* **2003**, *42*, 864.
21. Kunapuli, P.; Chitta, K. S.; Cowell, J. K. *Oncogene* **2003**, *22*, 3985.
22. Wei, Y.; Eble, J. A.; Wang, Z.; Kreidberg, J. A.; Chapman, H. A. *Mol. Biol. Cell* **2001**, *12*, 2975.
23. Wei, Y.; Waltz, D. A.; Rao, N.; Drummond, R. J.; Rosenberg, S.; Chapman, H. A. *J. Biol. Chem.* **1994**, *269*, 32380.
24. Jacobsen, B.; Gardsvoll, H.; Juhl Funch, G.; Ostergaard, S.; Barkholt, V.; Ploug, M. *Protein Exp. Purif.* **2007**, *52*, 286.
25. Sutter, P. W. C. D. *J. Heterocycl. Chem.* **1982**, *19*, 997.
26. Nabar, U. T. K.; Sunthakar, S. V. *Indian J. Chem.* **1983**, *22B*, 812.
27. Gornostaev, L. M. D.; Titova, N. G.; Arnol'd, E. V.; Lavrikova, T. I. *Russ. J. Org. Chem.* **2006**, *42*, 1364.
28. Wang, F.; Eric Knabe, W.; Li, L.; Jo, I.; Mani, T.; Roehm, H.; Oh, K.; Li, J.; Khanna, M.; Meroueh, S. O. *Bioorg. Med. Chem.* **2012**, *20*, 4760.
29. Zhong, S.; Chen, X.; Zhu, X.; Dziegielewska, B.; Bachman, K. E.; Ellenberger, T.; Ballin, J. D.; Wilson, G. M.; Tomkinson, A. E.; MacKerell, A. D. *J. Med. Chem.* **2008**, *51*, 4553.
30. Tarui, T.; Andronicos, N.; Czekay, R. P.; Mazar, A. P.; Bdeir, K.; Parry, G. C.; Kuo, A.; Loskutoff, D. J.; Cines, D. B.; Takada, Y. *J. Biol. Chem.* **2003**, *278*, 29863.
31. Bass, R.; Ellis, V. *Thromb. Haemost.* **2009**, *101*, 954.
32. Liu, D.; Aguirre Ghiso, J.; Estrada, Y.; Ossowski, L. *Cancer Cell* **2002**, *1*, 445.
33. Simon, D. I.; Wei, Y.; Zhang, L.; Rao, N. K.; Xu, H.; Chen, Z. P.; Liu, Q. M.; Rosenberg, S.; Chapman, H. A. *J. Biol. Chem.* **2000**, *275*, 10228.
34. Wei, Y.; Tang, C. H.; Kim, Y.; Robillard, L.; Zhang, F.; Kugler, M. C.; Chapman, H. A. *J. Biol. Chem.* **2007**, *282*, 3929.
35. Gardsvoll, H.; Jacobsen, B.; Kriegbaum, M. C.; Behrendt, N.; Engelholm, L.; Ostergaard, S.; Ploug, M. *J. Biol. Chem.* **2011**, *286*, 33544.
36. Mertens, H. D.; Kjaergaard, M.; Mysling, S.; Gardsvoll, H.; Jorgensen, T. J.; Svergun, D. I.; Ploug, M. *J. Biol. Chem.* **2012**, *287*, 34304.
37. Huai, Q.; Mazar, A. P.; Kuo, A.; Parry, G. C.; Shaw, D. E.; Callahan, J.; Li, Y. D.; Yuan, C.; Bian, C. B.; Chen, L. Q.; Furie, B.; Furie, B. C.; Cines, D. B.; Huang, M. D. *Science* **2006**, *311*, 656.
38. Tang, M. L.; Vararattanavech, A.; Tan, S. M. *J. Biol. Chem.* **2008**, *283*, 25392.
39. Patel, J. B.; Appaiah, H. N.; Burnett, R. M.; Bhat-Nakshatri, P.; Wang, G.; Mehta, R.; Badve, S.; Thomson, M. J.; Hammond, S.; Steeg, P.; Liu, Y.; Nakshatri, H. *Oncogene* **2011**, *30*, 1290.
40. Bugge, T. H.; Suh, T. T.; Flick, M. J.; Daugherty, C. C.; Romer, J.; Solberg, H.; Ellis, V.; Dano, K.; Degen, J. L. *J. Biol. Chem.* **1995**, *270*, 16886.
41. Solberg, H.; Ploug, M.; Hoyer-Hansen, G.; Nielsen, B. S.; Lund, L. R. *J. Histochem. Cytochem.* **2001**, *49*, 237.
42. Plesner, T.; Ralfkiaer, E.; Witttrup, M.; Johnsen, H.; Pyke, C.; Pedersen, T. L.; Hansen, N. E.; Dano, K. *Am. J. Clin. Pathol.* **1994**, *102*, 835.
43. Nykjaer, A.; Moller, B.; Todd, R. F., 3rd; Christensen, T.; Andreassen, P. A.; Gliemann, J.; Petersen, C. M. *J. Immunol.* **1994**, *152*, 505.
44. Jacobsen, B.; Ploug, M. *Curr. Med. Chem.* **2008**, *15*, 2559.
45. Smith, H. W.; Marshall, C. J. *Nat. Rev. Mol. Cell Biol.* **2010**, *11*, 23.